CANCER GENOMICS & PROTEOMICS *15*: 349-364 (2018)
doi:10.21873/cgp.20094

Whole-transcriptomic Profile of SK-MEL-3 Melanoma Cells Treated with the Histone Deacetylase Inhibitor: Trichostatin A

ELIZABETH A. MAZZIO and KARAM F.A. SOLIMAN

College of Pharmacy and Pharmaceutical Sciences, Florida A and M University, Tallahassee, FL, U.S.A.

Abstract. *Background: Malignant melanoma cells can rapidly acquire phenotypic properties making them resistant to radiation and mainline chemotherapies such as decarbonize or kinase inhibitors that target RAS-proto-oncogene independent auto-activated mitogen-activated protein kinases (MAPK)/through dual specificity mitogen-activated protein kinase (MEK). Both drug resistance and inherent transition from melanocytic nevi to malignant melanoma involve the overexpression of histone deacetylases (HDACs) and a B-Raf proto-oncogene (BRAF) mutation. Materials and Methods: In this work, the effects of an HDAC class I and II inhibitor trichostatin A (TSA) on the whole transcriptome of SK-MEL-3 cells carrying a BRAF mutation was examined. Results: The data obtained show that TSA was an extremely potent HDAC inhibitor within SK-MEL-3 nuclear lysates, where TSA was then optimized for appropriate sub-lethal concentrations for in vitro testing. The whole-transcriptome profile shows a basic phenotype dominance in the SK-MEL-3 cell line for i) synthesis of melanin, ii) phagosome acidification, iii) ATP hydrolysis-coupled proton pumps and iv) iron transport systems. While TSA did not affect the aforementioned major systems, it evoked a dramatic change to the transcriptome: reflected by a down-regulation of 810 transcripts and up-regulation of 833, with fold-change from –15.27 to +31.1 FC ($p<0.00001$). Largest differentials were found for the following transcripts: Up-regulated: Tetraspanin 13 (TSPAN13), serpin family i member 1 (SERPINI1), ATPase Na+/K+ transporting subunit beta 2 (ATP1B2), nicotinamide nucleotide adenylyl transferase 2 (NMNAT2), platelet-derived growth factor receptor-like (PDGFRL), cytochrome P450 family 1 subfamily A member 1 (CYP1A1), prostate androgen-regulated mucin-like protein 1 (PARM1), secretogranin II (SCG2), SYT11 (synaptotagmin 11), rhophilin associated tail protein 1 like (ROPN1L); down-regulated: polypeptide N-acetylgalactosaminyltransferase 3 (GALNT3), carbonic anhydrase 14 (CAXIV), BCL2-related protein A1 (BCL2A1), protein kinase C delta (PRKCD), transient receptor potential cation channel subfamily M member 1 (TRPM1), ubiquitin associated protein 1 like (UBAP1L), glutathione peroxidase 8 (GPX8), interleukin 16 (IL16), tumor protein p53 (TP53), and serpin family H member 1 (SERPINH1). There was no change to any of the HDAC transcripts (class I, II and IV), the sirtuin HDAC family (1-6) or the BRAF proto-oncogene v 599 transcripts. However, the data showed that TSA down-regulated influential transcripts that drive the BRAF–extracellular signal-regulated kinase (ERK)1/2 oncogenic pathway (namely PRKCD and MYC proto-oncogene which negatively affected the cell-cycle distribution. Mitotic inhibition was corroborated by functional pathway analysis and flow cytometry confirming halt at the G_2 phase, occurring in the absence of toxicity. Conclusion: TSA does not alter HDAC transcripts nor BRAF itself, but down-regulates critical components of the MAPK/MEK/BRAF oncogenic pathway, initiating a mitotic arrest.*

Correspondence to: Karam F.A. Soliman, Ph.D., College of Pharmacy & Pharmaceutical Sciences, Florida A&M University, 1520 ML King Blvd, Tallahassee, FL 32307, USA. E-mail: karam.soliman@famu.edu

Key Words: Melanoma cells, SK-MEL-3, transcriptomic profile, histone deacetylase inhibitor, trichostatin A, BRAF mutation, MAPK/MEK/BRAF oncogenic pathway, mitotic arrest.

Aggressive melanomas are highly resistant to radiation and chemotherapy drugs such as dacarbazine, and account for fatal metastatic disease. B-Raf proto-oncogene (*BRAF*) somatic missense mutations within the kinase domain from a single substitution (V599E) account for a large majority of malignant cutaneous melanoma. (1) This mutation in melanoma is often found in the absence of an NRAS or KRAS mutationm, but renders autoactivation of the extracellular signal-regulated kinase (ERK)/mitogen-activated protein kinase (MAPK) cascade (2-4). Despite the attempted use of combination therapies including dual-specificity mitogen-activated protein kinase (MEK) inhibitors (*e.g.*, trametinib, and cobimetinib) or BRAF inhibitors (*e.g.*, vemurafenib and dabrafenib), there is

a high degree of relapse (5-9). At the root of this pervasive resistance could be epigenetic changes that enable tumor cells to survive toxic insults, including those incurred from chemotherapy drugs. Some of the main epigenetic controlling elements are histone deacetylases (HDACs), which remove acetyl groups from histone tails and cores that drive nucleosome-constrictive gene silencing [reviewed in (10)]. The overexpression of HDACs in melanoma is a characteristic of acquired chemotherapeutic resistance (11) and drugs that inhibit HDACs such as panobinostat, and vorinostat prevent resistance to mainline drugs such as dacarbazine (12) and sensitize melanoma to BRAF/MEK inhibitors (13-16). HDAC inhibitors are believed to impair tumor-survival systems ,in part, by reducing the expression of anti-apoptotic proteins [survivin, B-cell lymphoma-extra-large (BCL-XL), BCL2, myeloid cell leukemia sequence 1 protein (MCL1), X-linked inhibitor of apoptosis (XIAP)], while at the same time elevating expression of contributors to death such as BCL2-like protein 4 (BAX), BCL2-associated X, apoptosis regulator (BAK) (17), death receptors (DR4 and DR5) (18), and the cell-cycle inhibitor (CKDN1A) (11). In this study, we evaluated the effects of trichostatin A (TSA), a potent class 1 and II HDAC inhibitor on the whole-transcriptome profile of SK-MEL-3 human melanoma cells, which carry the BRAF V599E mutation (1).

Materials and Methods

Cell culture media, phosphate-buffered saline, 96-well plates, pipette tips, fetal bovine serum (FBS), Alamar Blue and penicillin/streptomycin, as well as general reagents and supplies were all purchased from Sigma-Aldrich Co. (St. Louis, MO, USA) and VWR International (Radnor, PA, USA). SK-MEL-3 cells (ATCC HTB-69) and McCoy's 5a Medium Modified were obtained from the American Type Culture Collection (Rockville, MD, USA). All microarray equipment, reagents, and materials were purchased from Affymetrix/Thermo Fisher (Waltham, MA, USA).

HDAC activity. Nuclear lysates from untreated SK-MEL-3 cells were extracted using the EpiQuik™ Nuclear Extraction Kit (Epigentek; Farmingdale, NY, USA) and used for kinetic HDAC activity assays (ab156064; Abcam, Cambridge, MA, USA) according to the manufacturer's guidelines. The data were acquired using a Synergy HTX Multi-Mode Reader (BioTek, Winooski, VT, USA) with excitation at 355/40 nm, emission at 460/40 nm, optics: top, and gain: 37. Data were acquired using Gen5™ Data Analysis Software 2.06.10 (BioTek).

Cell culture. SK-MEL-3 (ATCC # HTB-69) cells were cultured in 175 cm3 flasks using ATCCs-formulated McCoy's 5a Medium, supplemented with FBS (10%) and 100 U/ml penicillin G sodium/100 μg/ml streptomycin sulfate. Cells were grown at 37˚C in 95% atmosphere/5% CO_2 and sub-cultured every 3-5 days.

Cell viability assay. Alamar Blue cell assay was used to determine both 24-h viable cell count and 7-day cell proliferation. In this assay, viable cells reduce resazurin to resorufin, a compound detectable by fluorescence. Briefly, 96-well plates were seeded with cells at a density of 5×10^6 cells/mI (24-h) or 0.5×10^6 cells/mI (7-day). Cells were treated with or without TSA (0.05-25 μM) and cultured at 37˚C, in 5% CO_2 atmosphere. Alamar Blue (0.1 mg/ml in Hanks balanced salt solution [HBSS)] was added at 15% v/v to each well, and the plates were incubated for 6-8 h. Quantitative analysis of dye conversion was measured by Synergy™ HTX Multi-Mode microplate reader (BioTek) at 550nm/580nm (excitation/emission). The data were expressed as viable cell count as a percentage of untreated controls.

Fluorescence microscopy. Actin staining was conducted on untreated controls *vs.* cells treated with 1.56 μM TSA for 24 h. Staining was achieved using Alexa Fluor 488® phalloidin (Thermofisher, Norcross, GA, USA) and images were obtained using a fluorescent/inverted microscope, CCD camera and data acquisition by ToupTek View (ToupTek Photonics Co, Zhejiang, P.R. China).

Whole-transcriptome human 2.1ST arrays. After treatment (1 μM of TSA *vs.* untreated controls) for 24 h, cells were washed three times in HBSS, followed by rapid freezing and storage at –80˚C. Using the basic trizol/chloroform method for RNA extraction led to failure at several quality control points, where it was determined that melanin appeared to be bound to the RNA and directly inhibited polymerase chain reactions. Consequently, total RNA was isolated and purified using Aurum total RNA mini kit (Bio-Rad, Hercules, CA, USA) which was effective in removal of melanin. Next, the whole-transcriptome analysis was conducted using preparation and instructions according to the GeneChipTM WT PLUS Reagent Manual for the human ST 2.1 array chips (Affymetrix/ThermoFisher Scientific, Waltham, MA, USA). Briefly, RNA was synthesized to first-strand cDNA, second-strand cDNA, followed by transcription to cRNA. cRNA was purified and assessed for yield, before synthesis of second-cycle single-stranded cDNA, hydrolysis of RNA and purification of second-cycle single-stranded cDNA. cDNA was then quantified for yield and equalized to 176 ng/ml. Subsequently, cDNA was fragmented, labeled, and hybridized onto the arrays before being subject to fluidics and imaging using the Gene Atlas (Affymetrix/ThermoFisher Scientific, Waltham, MA, USA). The array data quality control and initial processing from CEL to CHP files were conducted using expression console, before data evaluation using the Affymetrix transcriptome analysis console. The data were reported as fold change of TSA-treated cells relative to the control group.

Flow cytometry for cell-cycle phase determination. Cells were plated in 75 cm3 flasks and cultured in low serum media (0.5% FBS) for 24 h to synchronize cells in the cell cycle. After 24 h, low serum media was removed, and high serum culture media (10% FBS) was added before treatment with TSA. After 24 h, cells were trypsinized, centrifuged and washed twice with assay buffer (Cayman Chemical, Ann Arbor, MI, USA), re-suspended to a density of 106 cells/ml in a cell suspension, fixed and stored at –20˚C. After 48 h, the suspension was centrifuged at 300 × *g* for 2 min, the fixative was removed, and the pellet was re-suspended in 0.5 ml of staining solution containing propidium iodide (PI) and RNase A (Cayman Chemical). The distribution of DNA in all cell-cycle phases was assayed in replicates, and the proportion of cells in each stage was determined within 2 h by using a FACS Calibur flow cytometer (BD Biosciences, San Jose, CA, USA). For each sample, a total of 20,000 individual events from the gated subpopulation were analyzed separately. CellQuest Pro software

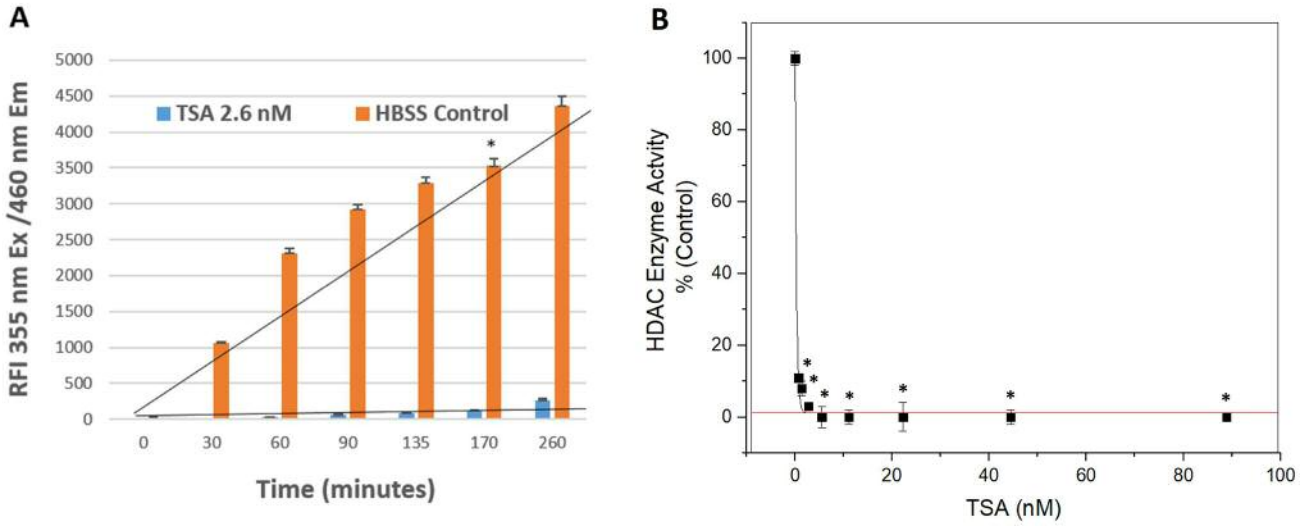

Figure 1. *Histone deacetylase (HDAC) kinetics in nuclear lysate from SK-MEL-3 cells. A: The data represent the formation of de-acetylated peptides over 260 min in the absence and presence of 2.6 nM trichostatin A (TSA). The data are expressed as the mean±S.E.M relative fluorescent units (RFU) (n=4). Significance between the two groups was quantified with a two-way ANOVA, where the between-groups significance was p<0.001. B: SK-MEL-3 HDAC enzyme inhibition by TSA at 170 min of incubation. The data represent SK-MEL-3 HDAC activity as a percentage of the control and are presented as the mean±S.E.M (n=4). The significance of the difference between the control and treatment groups was quantified by a one-way ANOVA and Tukey post-hoc test. *Significantly different from the control at p<0.001.*

(BD Biosciences) was used for acquisition and analysis of the data, and the percentage of cells in each phase was determined using ModFit LT 3.2.1 Software (Verity Software House. Topsham, ME, USA).

Data analysis. Statistical analysis was performed using Graph Pad Prism (version 3.0; Graph Pad Software Inc. San Diego, CA, USA) with the significance of the difference between the groups assessed using a one-way ANOVA followed by Tukey *post-hoc* means comparison test or Student's *t*-test. Microarray data were analyzed using Affymetrix expression console, transcription analysis software – incorporating analysis from the Database for Annotation, Visualization and Integrated Discovery (DAVID) v6.8 (19).

Results

TSA-mediated reduction of HDAC enzyme activity. Nuclear HDAC activity in SK-MEL-3 cells was confirmed by monitoring de-acetylated peptide formation as relative fluorescence, in the presence and absence of TSA (2.6 nM) over time (Figure 1A). Significant signal/noise at 37˚C was achieved at approximately 170 min of incubation, a time-point selected to generate a dose–response inhibition curve for TSA. The data show that the half maximal inhibitory concentration (IC_{50}) for TSA HDAC inhibition is less than 690 pM, which is extremely potent (Figure 1B). The SK-MEL3 HDAC nuclear lysate solution produced approximately 269 nM of deacetylated peptide product at 170 min under assay conditions (Figure 2A), as quantified according to the de-acetylated peptide standard curve. Figure 2B represents the time course for the formation of a fluorometric product from the de-acetylated peptide product using the developer solution (lysl endopeptidase). TSA did not interfere with the product developer solution (Figure 2B), showing specificity only for the inhibition of HDAC (Figure 1).

Cytotoxicity of TSA. 24-hour toxicity of TSA in SK-MEL-3 cells was conducted where the data show a relatively high-dose sub-lethal concentration yielding no observable effects on cell viability (Figure 3A) or structural morphology (Figure 3B) at 1.56 nM of TSA. A 7-day proliferation study was also conducted at the same concentrations, where the data show TSA to exert cytostatic effects similar to the negative taxol control (1 μM) (Figure 3A). These findings clearly show a predominant effect on the cell cycle, rather than apoptosis.

Such a high concentration of melanin in SK-MEL-3 cells completely blocked all *in vitro* transcription and PCR amplification processes using the standard trizol/chloroform technique of RNA extraction. Therefore, after 24 h of treatment with 1 μM TSA, total RNA was extracted using steps essential to remove melanin from the nucleotide component using a spin-column technique. Basic array analysis on the control cells set showed a basic phenotype of SK-MEL-3 cells (Table I) with the inherent dominance of melanin synthesis, phagosome acidification, ATP hydrolysis-coupled proton and iron transport, where these systems remained largely unaffected by TSA.

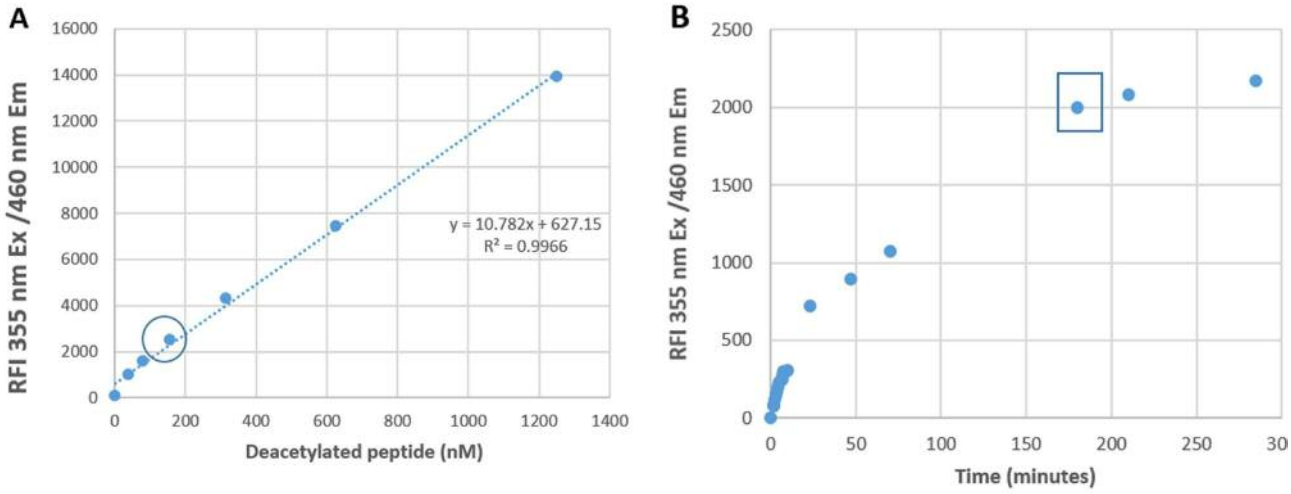

Figure 2. *Histone deacetylase (HDAC) kinetics in nuclear lysate from SK-MEL-3 cells A: The de-acetylated peptide standard curve was generated using the endopeptidase fluorometric detection solution at 170 min. Using this point of reference, the nuclear HDAC enzyme capacity of SK-MEL-3 cells for product formation was 156 nM (denoted by encircled data point). B: Kinetics of HDAC secondary cascade reaction –involving product detection and fluoro-probe production. The data represent a single concentration of de-acetylated peptide (156 nM) cleaved through endopeptidase to form a fluorometric product. These findings show that HDAC substrate conversion to the product is a time-dependent process that parallels conversion of the HDAC substrate to product.*

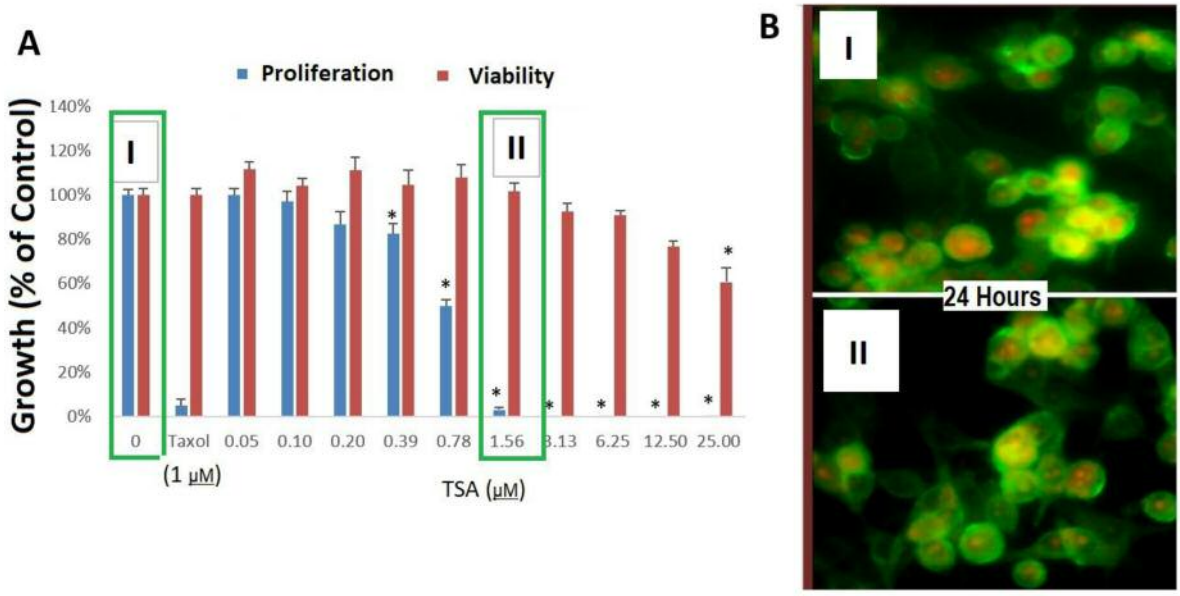

Figure 3. *Effects of trichostatin A (TSA) on SK-MEL-3 melanoma cell growth. A: Viability (at 24 h) and cell proliferation (at 7 days) as a percentage that of the control and compared with the negative control taxol. Data are presented as the mean±SEM (n=4). The significance of the difference between the control and treatment groups was quantified by a one-way ANOVA and Tukey post-hoc test. *Significantly different from the control at p<0.05. B: There were no observable differences in morphology or actin structure at the chosen concentration of TSA (1.56 μM) vs. controls.*

In contrast, there were enormous changes to the whole-transcriptome evoked by TSA which is reflected by the volcano plot with highlighted gene symbols shown in Figure 4; most dominant changes are also presented in Table II, with data available for downloading at NCBI's Gene Expression Omnibus accessible through GEO Series accession number GSE104265 (https://www.ncbi.nlm.nih.gov/geo/query/acc.cgi? acc=GSE104265). In brief, the information provides

Table I. *Global transcriptomic profile by dominant processes within SK-MEL-3 (ATCC® HTB-69™) cells which were derived from a metastatic site (lymph node) from a 42-year-old Caucasian female with malignant melanoma. Data were acquired using the PANTHER (Protein ANalysis THrough Evolutionary Relationships) Classification System (61, 62).*

GO biological process complete	No. of genes studied	Altered genes		Fold enrichment	*p*-Value
		No. found	No. expected		
Melanin biosynthetic process	13	6	0.19	32.1	4.14E–04
Melanin metabolic process	14	6	0.2	29.8	6.39E–04
Metabolic process	9916	191	142.59	1.34	1.33E–04
Organic substance metabolic process	9468	187	136.15	1.37	2.62E–05
Cellular metabolic process	8976	180	129.07	1.39	2.43E–05
Cellular process	14970	271	215.26	1.26	5.08E–11
Organic hydroxy compound biosynthetic process	153	13	2.2	5.91	4.27E–03
Secondary metabolite biosynthetic process	16	6	0.23	26.08	1.39E–03
Phagosome acidification	27	8	0.39	20.61	7.17E–05
Phagosome maturation	40	8	0.58	13.91	1.42E–03
Organelle organization	3129	82	44.99	1.82	2.47E–04
Cellular component organization	5261	127	75.65	1.68	6.98E–07
Cellular component organization or biogenesis	5484	137	78.86	1.74	3.99E–09
Intracellular pH reduction	45	9	0.65	13.91	2.38E–04
Regulation of intracellular pH	92	12	1.32	9.07	1.28E–04
Regulation of cellular pH	96	12	1.38	8.69	2.03E–04
Regulation of pH	103	14	1.48	9.45	4.76E–06
Monovalent inorganic cation homeostasis	132	14	1.9	7.38	1.06E–04
Cation homeostasis	633	26	9.1	2.86	1.91E–02
Inorganic ion homeostasis	648	26	9.32	2.79	2.89E–02
Cellular monovalent inorganic cation homeostasis	110	12	1.58	7.59	8.71E–04
Cellular cation homeostasis	569	25	8.18	3.06	9.28E–03
Cellular ion homeostasis	584	25	8.4	2.98	1.47E–02
ATP-coupled proton transport	27	7	0.39	18.03	1.52E–03
ATP hydrolysis-coupled cation transport	58	9	0.83	10.79	1.98E–03
Ion transport	1312	42	18.87	2.23	1.00E–02
Transport	4382	163	63.01	2.59	1.38E–32
Establishment of localization	4491	164	64.58	2.54	7.05E–32
Localization	5459	174	78.5	2.22	3.67E–27
Transmembrane transport	1220	41	17.54	2.34	4.03E–03
ATP hydrolysis-coupled ion transport	70	9	1.01	8.94	9.28E–03
Energy coupled proton transport,	28	8	0.4	19.87	9.47E–05
Hydrogen ion transmembrane transport	116	13	1.67	7.79	1.87E–04
Proton transport	149	13	2.14	6.07	3.19E–03
Hydrogen transport	151	13	2.17	5.99	3.69E–03
Transferrin transport	36	8	0.52	15.45	6.41E–04
Protein transport	1358	71	19.53	3.64	1.42E–17
Peptide transport	1383	71	19.89	3.57	3.89E–17
Amide transport	1404	72	20.19	3.57	2.04E–17
Nitrogen compound transport	1667	83	23.97	3.46	4.83E–20
Organic substance transport	2030	93	29.19	3.19	1.35E–20
Ferric iron transport	39	8	0.56	14.27	1.17E–03
Iron ion transport	58	9	0.83	10.79	1.98E–03
Transition metal ion transport	110	11	1.58	6.95	6.90E–03
Trivalent inorganic cation transport	39	8	0.56	14.27	1.17E–03

analysis of 48,226 transcripts, of which 1,643 genes were differentially expressed: 833 genes were up-regulated, and 810 genes were down-regulated.

There was no differential change to HDACs (class I, II and IV) 1-12 (Figure 5) nor the sirtuin HDAC class (1-6) (data not shown), and similarly no change in transcript for mutated *BRAF* (data not shown).

Using the Affymetrix transcriptome console, major changes were found in three areas related to tumor control: MAPK signaling (Figure 6A), cell-cycle regulation (Figure 6B), with

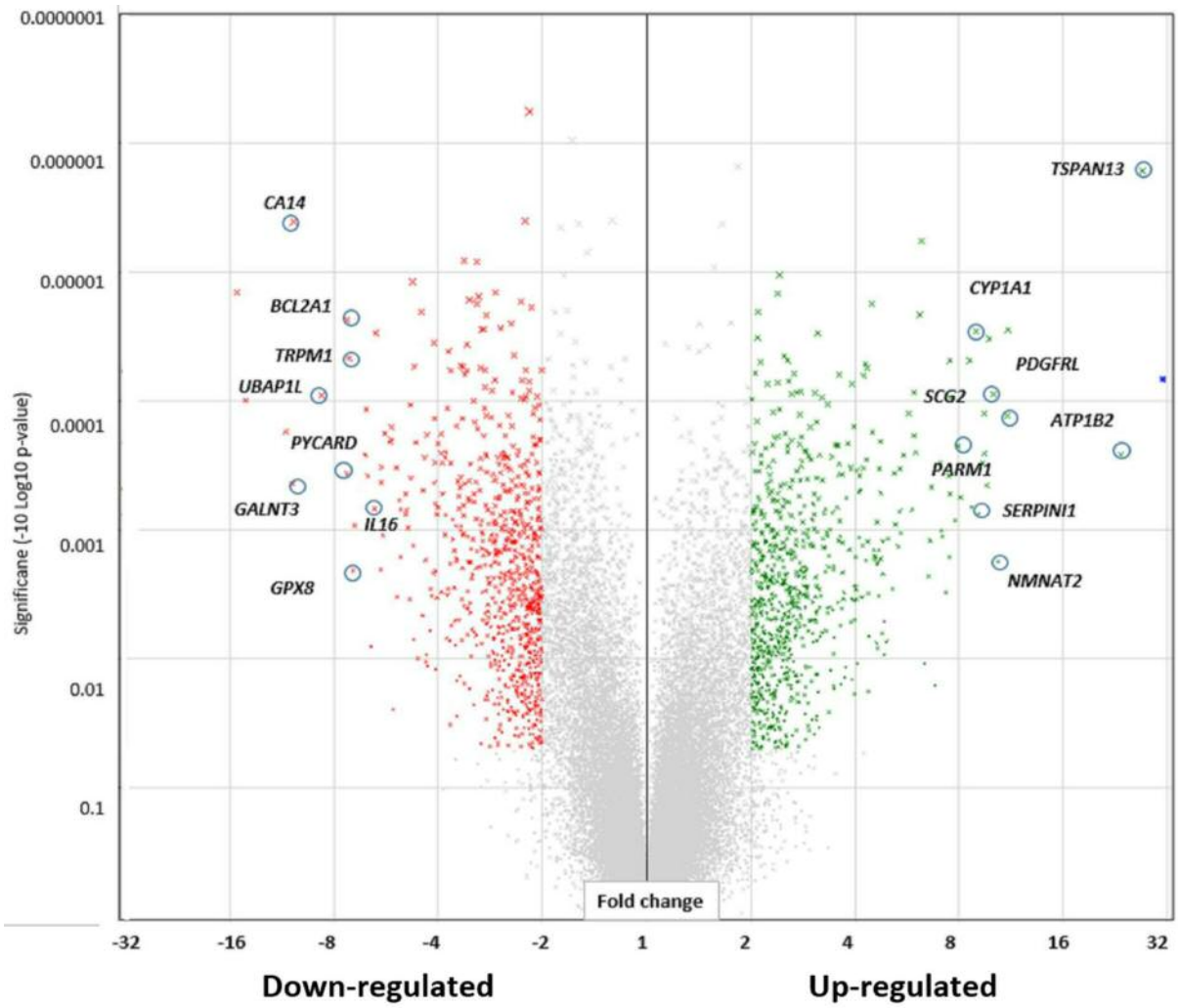

Figure 4. *Whole-transcriptome changes in trichostatin A (TSA)-treated cells using the GeneChip™ Human Gene 2.1 ST Array. The total number of genes tested was 48,226, of which 1,643 genes were differentially expressed: 833 were up-regulated, and 810 were down-regulated. These data are presented using a volcano plot (fold-change by significance). Down-regulated genes are shown in red and up-regulated genes in green; some of the most influential changes are highlighted. Genes are also listed in Table II. Down-regulated: Interleukin 16 (IL16), glutathione peroxidase (GPX8), ubiquitin associated protein 1-like (UBAP1L), PYD and CARD domain-containing (PYCARD), transient receptor potential cation channel (M1TRPM1), BCL2-related protein A1 (BCL2A1), carbonic anhydrase XIV (CA14), polypeptide N-acetylgalactosaminyltransferase 3 (GALNT3). Up-regulated: tetraspanin (13 TSPAN13), serpin peptidase inhibitor, clade I (neuroserpin; SERPINI1), ATPase, Na+/K+ transporting, beta 2 polypeptide (ATP1B2), nicotinamide nucleotide adenylyl transferase 2 (NMNAT2), platelet-derived growth factor receptor-like (PDGFRL), cytochrome P450, family 1, subfamily A, polypeptide (1CYP1A1), prostate androgen-regulated mucin-like protein 1 (PARM1), secretogranin II (SCG2).*

mitotic arrested also confirmed by flow cytometry (Figure 6C) and apoptosis (Figure 6D). In total, these findings demonstrate the global impact of inhibition of HDAC enzyme activity in SK-MEL3 malignant melanoma cells.

Discussion

Malignant melanoma can advance rapidly toward radiation and drug resistance, worsened by an inherent mutation of the *BRAF* gene which enables auto-activated RAF-independent oncogenic MAPK signaling. While there are dozens of *BRAF* mutations, the most common is a substitution at nucleotide 1799 where a mutation leads to valine being replaced by glutamate at codon 599 or 600. Treatment with inhibitors of BRAF (dabrafenib) or MEK (trametinib) can be initially effective, with time, there is often a high degree of relapse and development of resistance to chemotherapy agents (5-9).

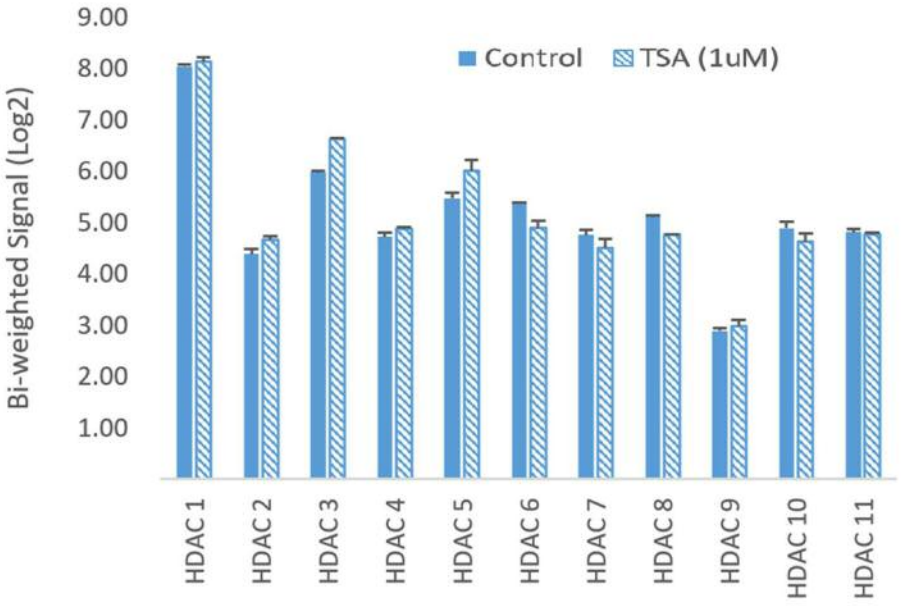

Figure 5. *Effects of trichostatin A (TSA) (1 μM) treatment for 24 h on histone deacetylase (HDAC) transcripts. The data represent the mean±SEM of the log2 bi-weighted signal from whole-transcriptome arrays. There were no significant differences between the two groups.*

The epigenetic events which contribute to chemoresistant phenotypes might offer therapeutic targets for combination drug strategies. Moreover, while there are thousands of biological epigenetic controls, HDACs function as high-capacity removers of acetyl groups from histones to sustain silencing. Epigenetic drugs that inhibit one or more HDACs can broadly alter the transcriptome by reactivating either coding or non-coding functional mRNAs which contribute to antitumor phenotypes (11). In the case of melanoma, combined therapy with HDAC inhibitors reportedly prevents resistance to dacarbazine (12) and sensitize melanoma to BRAF and MEK inhibitors (13-16), but the mechanism for this is not well understood. In addition, while there is potential for the use of HDACS of diverse types (*e.g.*, vorinostat, tubacin, sirtinol, vorinostat, suberoyl *bis*-hydroxamic acid) in the treatment of melanoma [review in (20)], HDAC inhibitors are broad-based, not specific to areas of the genome, and can elicit unwanted side-effects (11), such as hematological toxicity, fatigue and nausea (21).

Given the research community interest regarding the direct effects of HDAC inhibitors on *BRAF*-mutant melanoma, the goal of this investigation was to examine the efficacy of a known HDAC inhibitor (TSA) and its ability to alter the transcriptome in a *BRAF*-mutant melanoma cell model. While a discussion of the data in its entirety is not possible given the hundreds of changes to the transcriptome, furthermore there are changes to many transcripts for which little is known, we briefly discuss changes relevant to BRAF signaling.

MAPK signaling. BRAF signaling in tumor cells is overactive corresponding to abnormally high levels of phosphorylation signaling. The data in this work confirm that TSA neither alters the transcription of several HDAC classes or the expression of *BRAF* itself. In contrast, TSA was found to reduce transcript levels of controlling elements of BRAF signaling, namely the upstream target protein kinase C delta (*PRKCD*) and downstream target *MYC*. *PRKCD* is upstream of *BRAF* and is highly overexpressed in a number of types of aggressive metastatic cancer (22) being an activator of phospho-ERK 1/2 signaling which can drive chemoresistant tumors (23-25), unbridled cell proliferation (22), phosphorylation of E-cadherin (which can perpetuate metastasis) (26) and in hypoxic tumors, up-regulate mRNA levels of hypoxia-inducible factor 1 alpha (HIF1α) (27) and glucose metabolism (28). The TSA-mediated reduction in *MYC* is one of the most compelling targets for treating chemoresistant melanoma. Down-regulation of MYC alone essentially blocks all four oncogenic pathways which lead to its up-regulation, namely NRAS proto-oncogene, GTPase (NRAS), BRAF, phosphatidylinositol-3-kinase and NOTCH (29), which are driving elements of MYC-directed tumor initiation, maintenance, and metastasis (30). Analysis of a large data pool of patient-derived *BRAF*-mutant melanoma showed that several pathways singly converge on activated overexpressed MYC, which manifests itself during relapse, resistance to BRAF/MEK inhibitors (29, 31, 32) and transition of normal human skin to dysplastic nevi (33). The transformative

Table II. *Differentially expressed transcripts in trichostatin A (TSA)-treated vs. control-untreated SK-MEL-3 cells. The data are expressed as fold change (FC) and level of significance represented by a p-Value and false discovery rate (FDR) adjusted p-value.*

Gene symbol	Description	Mean bi-weighted. signal (log2)			*p*-Value	FDR *p*-value
		Ctrl	TSA	Fold-change		
TSPAN13	**Tetraspanin 13**	4.50	9.26	**27.1**	2.0E−06	0.020
SERPINI1	**Serpin peptidase inhibitor, clade I (neuroserpin)**	3.42	7.98	**23.5**	2.6E−04	0.046
ATP1B2	**ATPase, Na+/K+ transporting, beta 2 polypeptide**	3.65	7.11	**11.0**	1.3E−04	0.041
NMNAT2	**Nicotinamide nucleotide adenylyl transferase 2**	3.04	6.41	**10.4**	1.8E−03	0.072
PDGFRL	**Platelet-derived growth factor receptor-like**	4.56	7.89	**10.1**	8.8E−05	0.038
CYP1A1	Cytochrome P450, family 1, subfamily A, polypeptide 1	3.60	6.88	**9.8**	3.3E−05	0.032
PARM1	Prostate androgen-regulated mucin-like protein 1	4.46	7.73	**9.6**	4.5E−04	0.050
ROPN1L	Rhoephilin associated tail protein 1-like	2.80	6.04	**9.5**	1.3E−04	0.041
SCG2	Secretogranin II	3.87	7.11	**9.5**	2.6E−04	0.046
SYT11	Synaptotagmin XI	6.21	9.43	**9.4**	3.0E−04	0.047
HIST1H2AG	Histone cluster 1, H2ag	3.74	6.93	**9.1**	7.5E−04	0.057
CTGF	Connective tissue growth factor	3.57	6.73	**9.0**	2.9E−05	0.030
SYN1	Synapsin I	3.85	6.97	**8.7**	6.7E−04	0.056
DNER	Delta/NOTCH like EGF repeat containing	5.52	8.62	**8.6**	4.8E−05	0.034
FABP4	Fatty acid binding protein 4, adipocyte	1.79	4.80	**8.1**	5.6E−04	0.052
STC1	Stanniocalcin 1	2.46	5.46	**8.0**	2.2E−04	0.045
EFNB2	Ephrin-B2	3.06	6.03	**7.8**	8.5E−04	0.060
SRXN1	Sulfiredoxin 1	7.18	10.10	**7.6**	9.6E−05	0.039
CYFIP2	cytoplasmic FMR1 interacting protein 2	4.43	7.34	**7.5**	4.9E−05	0.034
SLC7A11	solute carrier family 7	6.85	9.75	**7.5**	5.3E−04	0.051
SEMA3D	Semaphorin 3D	3.16	6.07	**7.5**	1.6E−03	0.072
ELOVL4	ELOVL fatty acid elongase 4	3.82	6.72	**7.5**	3.8E−04	0.048
GUSBP3	Glucuronidase, beta pseudogene 3	3.50	6.37	**7.3**	3.1E−03	0.090
MIR2909	MicroRNA 2909	6.36	9.21	**7.2**	1.1E−03	0.064
ID1	Inhibitor of DNA binding 1	3.97	6.80	**7.1**	1.0E−03	0.063
TMEM47	Transmembrane protein 47	4.65	7.47	**7.1**	3.0E−04	0.047
CXADR; BTG3	Coxsackie virus and adenovirus receptor	4.59	7.36	**6.8**	1.6E−02	0.171
SPTLC3	Serine palmitoyltransferase, long chain base subunit 3	4.88	7.61	**6.6**	4.7E−04	0.050
VGF	VGF nerve growth factor inducible	4.75	7.47	**6.6**	1.2E−03	0.066
EID3	EP300 interacting inhibitor of differentiation 3	4.28	6.99	**6.6**	2.3E−03	0.080
BASP1	Brain-abundant, membrane-attached signal protein 1	4.01	6.68	**6.4**	1.1E−02	0.142
LOC730101	uncharacterized LOC730101	4.51	7.14	**6.2**	6.0E−06	0.025
ATP8A1	ATPase, aminophospholipid transporter (APLT)	3.60	6.22	**6.2**	2.1E−05	0.029
CYR61	Cysteine-rich, angiogenic inducer, 61	4.37	6.94	**5.9**	8.5E−05	0.038
PCDH9	Protocadherin 9	3.33	5.90	**5.9**	1.9E−04	0.044
PRKAR2B	Protein kinase, cAMP-dependent, reg 2B	5.08	7.63	**5.9**	7.0E−04	0.056
EFNA3	Ephrin-A3	3.75	6.27	**5.7**	1.3E−04	0.041
HIST2H4B; 4A	Histone cluster 2, H4b; histone cluster 2, H4a	5.87	8.34	**5.5**	2.7E−04	0.046
ATP1B1	ATPase, Na+/K+ transporting, beta 1 polypeptide	4.81	7.24	**5.4**	1.1E−03	0.063
MYCT1	MYC target 1	2.68	5.12	**5.4**	3.4E−04	0.047
SSBP2	Single-stranded DNA binding protein 2	4.46	6.89	**5.4**	7.2E−04	0.056
STK17A	Serine/threonine kinase 17a	5.65	8.07	**5.4**	1.4E−03	0.068
ANXA1	Annexin A1	5.69	8.07	**5.2**	3.7E−04	0.048
PEG10	Paternally expressed 10	7.65	10.01	**5.1**	2.9E−03	0.087
HMOX1	Heme oxygenase 1	6.13	8.45	**5.0**	1.2E−03	0.065

Table II. *Continued*

SLC9A7	Solute carrier family 9, subfamily A (NHE7)	2.61	4.92	**4.9**	7.4E−03	0.122
LIFR	Leukemia inhibitory factor receptor alpha	2.33	4.60	**4.9**	5.2E−03	0.108
DHRS2	Dehydrogenase/reductase (SDR family) member 2	2.61	4.89	**4.8**	9.3E−03	0.133
NLRP1	NLR family, pyrin domain containing 1	5.98	8.25	**4.8**	1.2E−03	0.066
RALGAPA2	Ral GTPase activating protein, as2	5.89	8.15	**4.8**	2.2E−03	0.079
B3GALT1	UDP-Gal: betaGlcNAc beta 1,3-galactosyltransferase 1	2.75	5.01	**4.8**	6.4E−03	0.116
ST8SIA4	ST8 alpha-*N*-acetyl-neuraminide sialyltransferase 4	4.90	7.15	**4.8**	5.2E−04	0.051
PRDX1	Peroxiredoxin 1	5.50	7.75	**4.8**	1.7E−03	0.072
ACTBL2	Actin, beta-like 2	2.45	4.70	**4.7**	2.1E−04	0.045
ENPP2	Ectonucleotide pyrophosphatase/phosphodiesterase 2	6.91	9.15	**4.7**	3.4E−04	0.047
PELI1	Pellino E3 ubiquitin protein ligase 1	5.64	7.87	**4.7**	1.4E−03	0.070
SMIM10L2B	Small integral membrane protein 10 like 2B	2.76	4.98	**4.7**	3.3E−03	0.092
MAP2	Microtubule associated protein 2	3.65	5.87	**4.7**	1.8E−03	0.073
SLC41A2	Solute carrier family 41 (magnesium transporter), member 2	3.86	6.07	**4.7**	8.3E−03	0.127
PAIP2B	Poly(A) binding protein interacting protein 2B	5.01	7.22	**4.6**	1.9E−03	0.074
UNC5D	Unc-5 netrin receptor D	2.90	5.11	**4.6**	8.7E−04	0.060
PRKAA2	Protein kinase, AMP-activated, alpha 2 catalytic subunit	4.15	6.36	**4.6**	7.6E−03	0.123
TTLL7	Tubulin tyrosine ligase-like family member 7	5.18	7.37	**4.6**	1.6E−03	0.072
USP53	Ubiquitin specific peptidase 53	5.73	7.92	**4.6**	1.6E−03	0.072
MGAT4A	Mannosyl glycoprotein *n*-acetylglucosaminyltransferase	3.13	5.31	**4.5**	1.4E−03	0.070
CRIM1	Cysteine rich transmembrane bmp regulator 1 (chordin-like)	4.40	6.57	**4.5**	1.7E−03	0.072
SEL1L3	Sel-1 suppressor of lin-12-like 3 (*C. elegans)*	3.60	5.77	**4.5**	1.8E−04	0.044
SLC2A3	Solute carrier family 2	3.93	6.09	**4.5**	1.8E−05	0.029
MYEF2	Myelin expression factor 2	4.15	6.27	**4.4**	3.2E−03	0.090
HPSE	Heparanase	3.62	5.74	**4.4**	1.2E−03	0.066
LIPH	Lipase, member h	2.39	4.50	**4.3**	5.6E−05	0.034
DNAJB4	DNAJ (hsp40) homolog, subfamily b, member 4	4.56	6.67	**4.3**	2.9E−04	0.046
GCLM	Glutamate-cysteine ligase, modifier subunit	6.12	8.23	**4.3**	1.7E−03	0.072
MXD1	Max dimerization protein 1	5.10	7.20	**4.3**	5.2E−05	0.034
BCO2	Beta-carotene oxygenase 2	3.07	5.15	**4.2**	3.3E−04	0.047
EYA1	EYA transcriptional coactivator and phosphatase 1	4.89	6.96	**4.2**	1.3E−03	0.068
CDH19	Cadherin 19, type 2	5.30	7.37	**4.2**	3.4E−03	0.092
ENPP1	Ectonucleotide pyrophosphatase/phosphodiesterase 1	7.61	9.66	**4.1**	3.8E−04	0.048
ARRDC4	Arrestin domain containing 4	5.28	7.32	**4.1**	4.9E−04	0.050
ABCD2	ATP binding cassette subfamily d member 2	2.26	4.30	**4.1**	5.1E−04	0.051
EGR1	Early growth response 1	3.73	5.77	**4.1**	1.2E−03	0.065
FREM2	Fras1 related extracellular matrix protein 2	3.19	5.21	**4.1**	3.5E−04	0.047
HIST1H2BD	Histone cluster 1, H2bd	3.39	5.41	**4.1**	2.8E−03	0.086
ARHGAP29	Rho GTPase activating protein 29	3.25	5.27	**4.0**	3.5E−03	0.093
MGAM2	Maltase-glucoamylase 2 (putative)	3.78	5.79	**4.0**	2.9E−03	0.087
AHR	Aryl hydrocarbon receptor	8.63	10.64	**4.0**	1.6E−03	0.072
NPTX2	Neuronal pentraxin II	4.71	6.71	**4.0**	5.0E−03	0.107
MGAM2	Maltase-glucoamylase 2 (putative)	3.85	5.84	**4.0**	2.7E−03	0.086
TCN1	Transcobalamin I	3.20	5.19	**4.0**	3.5E−03	0.094
MGAM2	Maltase-glucoamylase 2 (putative)	2.81	4.80	**4.0**	1.9E−02	0.185
PRKCD	**Protein kinase C, delta**	**8.08**	**9.49**	**−2.6**	**3.61E−04**	**0.048**
PARP3	Poly (ADP-ribose) polymerase family member 3	7.11	5.11	**−4.0**	2.1E−04	0.045
ATOH8	Atonal bHLH transcription factor 8	5.74	3.73	**−4.0**	7.6E−04	0.057
ACAT2	Acetyl-CoA acetyltransferase 2	7.50	5.49	**−4.0**	3.4E−03	0.092
SNORD91B	Small nucleolar RNA, C/D box 91B	6.36	4.34	**−4.1**	1.2E−02	0.149
TRIP6	Thyroid hormone receptor interactor 6	7.80	5.77	**−4.1**	6.3E−04	0.055
TGFB1I1	Transforming growth factor beta 1 induced transcript 1	7.86	5.84	**−4.1**	2.1E−03	0.078

Table II. *Continued*

MYC	**v-myc Avian myelocytomatosis viral oncogene homolog**	**8.50**	**6.47**	**−4.1**	**1.4E−04**	**0.041**
PATZ1	POZ (BTB) and AT hook containing zinc finger 1	5.63	3.60	**−4.1**	4.3E−04	0.049
ZC3H7B	Zinc finger CCCH-type containing 7B	6.71	4.67	**−4.1**	3.5E−05	0.032
KCNJ13	Potassium channel, inwardly rectifying subfamily J	6.10	4.06	**−4.1**	2.2E−03	0.079
IGF2BP1	Insulin-like growth factor 2 mRNA binding protein 1	6.59	4.54	**−4.2**	3.3E−03	0.092
RFTN2	RAFTLIN family member 2	5.98	3.90	**−4.2**	2.9E−03	0.087
PRKG2	protein kinase, cGMP-dependent, type II	6.26	4.18	**−4.2**	6.1E−03	0.114
PHF19	PHD finger protein 19	6.29	4.19	**−4.3**	1.1E−02	0.145
ARHGAP31	Rho GTPase activating protein 31	6.01	3.90	**−4.3**	1.8E−04	0.044
MMP14	Matrix metallopeptidase 14 (membrane-inserted)	8.69	6.57	**−4.4**	2.8E−04	0.046
SLC45A2	Solute carrier family 45, member 2	9.67	7.52	**−4.4**	4.9E−04	0.050
MIR3142	microRNA 3142	6.19	4.04	**−4.4**	4.7E−03	0.103
MEPCE	Methylphosphate capping enzyme	7.15	4.99	**−4.5**	2.0E−05	0.029
NFATC2	Nuclear factor of activated T-cells	8.94	6.71	**−4.7**	5.4E−05	0.034
CXCL1	CXC ligand 1 (melanoma growth stimulating activity, alpha)	6.05	3.81	**−4.7**	1.2E−05	0.029
TEAD2	TEA domain family member 2	5.62	3.38	**−4.7**	1.3E−03	0.068
SLC24A5	Solute carrier family 24, member 5	9.18	6.92	**−4.8**	1.1E−04	0.039
GYPC	Glycophorin C (Gerbich blood group)	6.56	4.30	**−4.8**	4.0E−04	0.048
PER3	Period circadian clock 3	6.22	3.93	**−4.9**	9.7E−04	0.063
ANGPTL2	**Angiopoietin like 2**	**7.23**	**4.93**	**−4.9**	**7.1E−04**	**0.056**
OAS2	2-5-Oligoadenylate synthetase 2	6.66	4.35	**−5.0**	5.3E−04	0.051
HAS2	Hyaluronan synthase 2	6.72	4.41	**−5.0**	7.6E−04	0.057
ZBTB2	Zinc finger and BTB domain containing 2	6.30	3.94	**−5.1**	6.9E−04	0.056
LGI3	Leucine-rich repeat LGI family, member 3	9.08	6.71	**−5.2**	5.9E−04	0.053
HIST1H2BM	Histone cluster 1, H2bm	7.25	4.85	**−5.3**	3.3E−03	0.092
UCN2; PFKFB4	Urocortin 2	7.58	5.17	**−5.3**	3.3E−04	0.047
SNORA72	Small nucleolar RNA, H/ACA box 72	5.30	2.87	**−5.4**	2.5E−02	0.209
LCP2	Lymphocyte cytosolic protein 2	7.46	5.00	**−5.5**	2.0E−04	0.044
SPR	Sepiapterin reductase	7.77	5.31	**−5.5**	2.1E−04	0.045
APOBEC3C	Apolipoprotein B mRNA editing enzyme, catalytic polypeptide-like 3C	9.26	6.75	**−5.7**	1.8E−04	0.044
MIR4534	MicroRNA 4534	7.40	4.87	**−5.8**	1.1E−03	0.064
FRG2DP	FSHD region gene 2 family, member D, pseudogene	7.72	5.18	**−5.8**	3.3E−04	0.047
MIR146A	MicroRNA 146a	7.81	5.27	**−5.8**	4.3E−04	0.049
TPCN2	Two pore segment channels 2	8.86	6.31	**−5.9**	2.0E−03	0.077
FXYD3	FXYD domain containing ion transport regulator 3	6.98	4.38	**−6.1**	3.0E−05	0.030
SERPINH1	Serpin peptidase inhibitor, clade H	7.66	5.05	**−6.1**	6.8E−04	0.056
LOC285000	Uncharacterized LOC285000	5.93	3.26	**−6.4**	3.8E−04	0.048
TP53	Tumor protein p53	8.64	5.95	**−6.5**	1.2E−04	0.040
IL16	Interleukin 16	6.60	3.90	**−6.5**	2.6E−04	0.046
SNORA75	Small nucleolar RNA, H/ACA box 75	7.98	5.17	**−7.0**	9.4E−04	0.062
GPX8	Glutathione peroxidase 8 (putative)	6.24	3.43	**−7.1**	2.1E−03	0.078
UBAP1L	Ubiquitin-associated protein 1 like	6.86	4.00	**−7.2**	4.7E−05	0.034
PYCARD	PYD and CARD domain containing	7.98	5.10	**−7.3**	3.7E−04	0.048
TRPM1	Transient receptor potential cation channel, M1	6.61	3.73	**−7.4**	2.4E−05	0.030
BCL2A1	**BCL2-related protein A1**	**8.62**	**5.50**	**−8.7**	**9.0E−05**	**0.038**
CA14	**Carbonic anhydrase XIV**	**8.19**	**4.80**	**−10.5**	**4.0E−06**	**0.022**
GALNT3	**Polypeptide *N*-acetylgalactosaminyltransferase 3**	6.85	3.44	**−10.6**	4.4E−04	0.050
LINC00681	**Long intergenic non-protein coding RNA 681**	8.77	4.84	**−15.3**	1.4E−05	0.029

resistance of *BRAF*-mutant melanoma is reversible by knockdown or drug inhibition of *MYC* alone (29, 34-36).

Mitosis. Functional pathway analysis shows that TSA reduced several controls over key cell cycle-related transcripts including: ataxia telangiectasia mutated serine/threonine kinase (*ATM*) that is activated by DNA damage during radiation, responsible for activation of checkpoint cell-cycle controlling kinase 2 (*CHK2*), which can further prevent cells from entering mitosis at the G_2/M phase, all of which is believed to maintain stability of the genome (37-39). While it is uncertain what role this would have in cancer growth, a loss of function of ATM is believed to render greater genomic instability, which in theory would augment effects of radio-or chemotherapies. TSA also evoked a loss in the F-box protein S-phase kinase-associated protein 2 (SKP2) which is part of the SKP1–Cullin1–F-box protein ubiquitin ligase complex responsible for the degradation of cyclin-dependent kinase inhibitor p21 (CIP1/WAF1) which halts the cycle at the S-phase (40). A loss of SKP2 would be detrimental in several aspects such as initiating degradation of tumor suppressor p27 and KIP1 accumulation of p21, which causes S-phase arrest, cell proliferation and aggressive oncogenic potential (41-43). Loss-of-function of the SKP-Cullin, F-box containing complex (SCF)/SKP2 and degradation of the cyclin inhibitor $p27^{KIP1}$ appear to be controlling factors in migration, inadequate growth arrest and invasion of diverse cancer types (42, 44). Recent work indicated that activated CDK2 and several of the polo-like kinases collaborate to phosphorylate G_2 checkpoint kinase (WEE1), which could promote its ubiquitination by SCF (beta-transducing repeat containing (beta-TRCP) and in this manner perpetuate feedback signals to reinforce cycle transition (45).

TSA also reduced transcripts of the cell division cycle protein 45 (CDC45), which is required for DNA synthesis during genome duplication. CDC45 is overexpressed in several types of tumor cell, where it responsible for sustaining rapid rounds of cell division, amplification of DNA replication, chromosomal loading and unwinding and DNA synthesis at the replication fork (46). These events then activate CDKs and Dbf4-dependent kinase (DDK) to allow continued binding of CDC45 and heterotetramer of Sld5, Psf1, Psf2,and Psf3 (GINS) required for the CDC45/MCM2–7/GINS complex, and initiation/elongation of DNA for replication by DNA polymerase (47, 48). Furthermore, TSA rendered considerable loss of expression of *CDK4*, endothelial differentiation-related factor 1 (*EDF1*) and *EDF3*, all of which play critical roles in the cell cycle at the G_1/S transition. CDK4 normally phosphorylates retinoblastoma protein (Rb) (49) causing its disassociation from E2F transcription factor, where E2F is then free to transcribe S-phase-promoting genes. Normally the Rb tumor suppressor restrains the cell cycle by binding E2F1, rendering its inability to transcribe E2F genes that encode many proteins involved with DNA replication. Down-regulation of CKD4 could leave more unphosphorylated Rb, and therefore halt the cell cycle at this point. Several studies show this where knockdown of *CDK4* or use of compounds that are involved with its reduction such as asiatic acid will induce G_0/G_1 phase arrest of the cells (49, 50). Alterations in any key target of the CDK–Rb machinery will disrupt cell-cycle regulation, this being a valuable target for chemotherapeutic drug development.

Apoptosis. While TSA itself has been reported to induce apoptosis, cell death was not observed in this study at concentrations where HDAC inhibition occurred (51, 52). In contrast, we found confounding evidence of opposing forces in apoptosis, with significant losses of both tumor suppressor (*TP53*) and oncogenes (*BCL2*). While we confirm the work of others in the loss of BCL2 commonly reported with HDAC inhibitors (51, 53), we also confirm the less-reported attenuation of p53 (20). In general, it appears that HDAC inhibitors mediate anti-mitotic effects which predominate at a lower concentration over apoptotic effects.

Carbonic anhydrase. New findings in this work show that TSA induced a large loss in carbonic anhydrase 14 (CAXIV; 10-fold change, $p<0.0001$). Human carbonic anhydrases (EC 4.2.1.1) types IX and XII are overexpressed in a variety of cancer types and play a large role in pH regulation required to drive metastasis and growth, with greater importance to solid hypoxic tumors (54). Drugs such as CAIX inhibitor FC16-670A or any other compound that can down-regulate carbonic anhydrases will inevitably reduce the capacity of tumor cells to maintain acid-base equilibrium and thereby deal a vital blow to cancer survival, growth and resistance (*e.g.*, sulfamides (acetazolamide) and coumarins (umbelliferon)) (55, 56). Combined efficacy of chemotherapy drug treatment is greater when combined with an inhibitor of carbonic acids, proton pumps (57), or HDACs (58), all of which could reduce tumor acidity.

Tetraspanin 13. Here we report the TSA-mediated up-regulation of tetraspanin 13 (TSP13; 27.1-fold change, $p<0.0001$), the ramifications of which have not been subject to much research. Sparse research on its role shows TSP13 to be a diagnostic marker for prostate cancer (59), where its expression is inversely correlated to Gleason score ($p=0.01$), and high levels correlate with favorable prognosis (60). The role of TSP13 in the oncogenic potential of melanoma will require further investigation.

Conclusion

This work provides a basic framework showing global transcriptomic changes using a pan-HDAC inhibitor in *BRAF*-mutant melanoma. The data provide evidence that

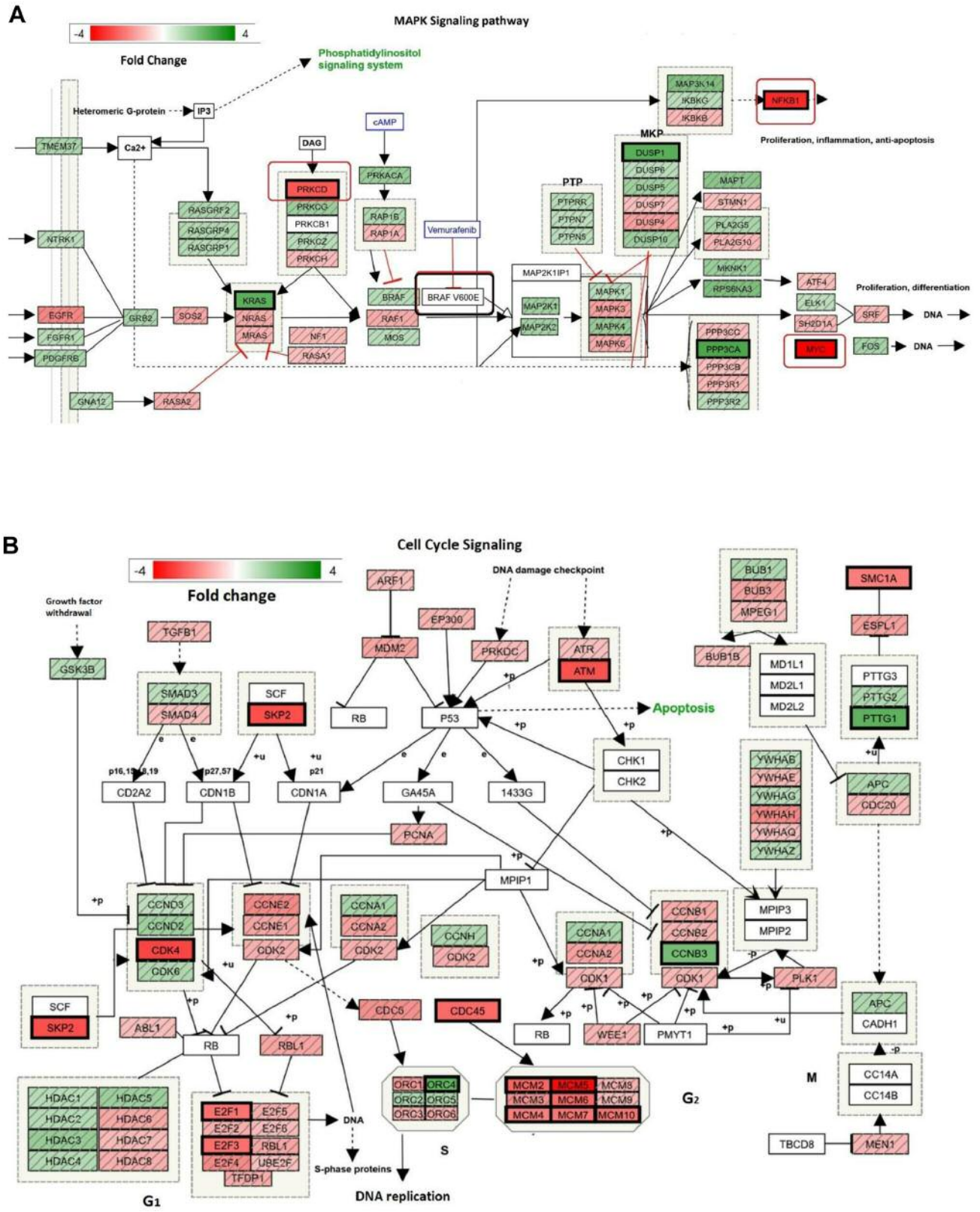

Figure 6. *Continued*

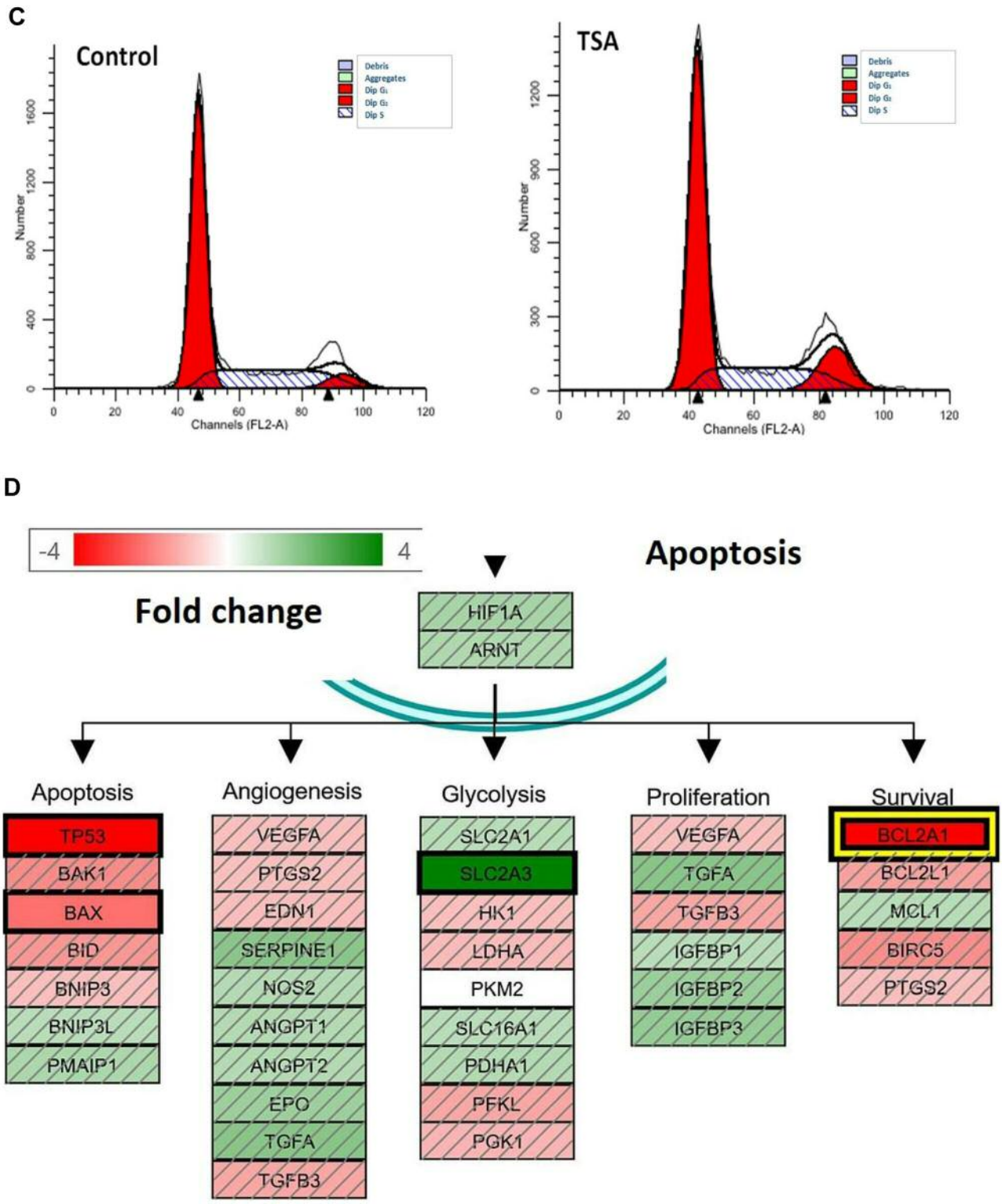

Figure 6. *Pathway analysis. Effects of histone deacetylase (HDAC) enzyme inhibition with trichostatin A (TSA) (1 μM) at 24 h on A: Mitogen-activated protein kinases (MAPK) signaling, B: cell-cycle signaling, C: cell-cycle distribution, and D: apoptosis. In C, representative cytograms are shown in the upper two panels; in the lower panel, the data represent the mean percentage of cells per phase (±SEM; n=4), and significance of differences from controls was determined with a t-test. *Significantly different at p<0.05.*

TSA while inhibiting HDAC enzyme activity, does not alter transcription of various classes of HDAC nor *BRAF* itself, but in fact down-regulates critical components of MAPK–MEK–/BRAF oncogenic pathways, initiating a mitotic arrest. Functional pathway analysis showed that TSA negatively affected cell cycle progression, with flow cytometry confirming a halt at the G_2 phase with no effect on apoptosis. The loss of anti-apoptotic *BCL2* juxtaposed on the loss of apoptotic *TP53* may account for the lack of toxicity observed in TSA-treated cells. These data provide a basis for further investigation as to the mechanisms of action for HDAC inhibition in *BRAF*-mutant malignant melanoma.

Data Sharing

The data discussed in this publication have been deposited in NCBI's Gene Expression Omnibus and are accessible through GEO Series accession number GSE102891 LOCATED AT https://www.ncbi.nlm.nih.gov/geo/query/acc.cgi?acc=GSE104265

Conflicts of Interest

The Authors confirm that there are no known conflicts of interest associated with this publication and there was no significant financial support for this work that could have influenced its outcome.

Acknowledgements

This project was supported by grants from the National Institutes of Health, National Institute on Minority Health and Health Disparities, RCMI grant (G12MD007582), COE grant (P20 MD006738) and the National Cancer Institute under grant number P50 CA168536, Moffitt Skin Cancer SPORE, CEP Program. The Authors would like to thank Dr. Ramesh Badisa, from Florida A & M University, College of Pharmacy and Pharmaceutical Sciences for his support in flow cytometry data acquisition and analysis.

References

1 Reifenberger J, Knobbe CB, Sterzinger AA, Blaschke B, Schulte KW, Ruzicka T and Reifenberger G: Frequent alterations of Ras signaling pathway genes in sporadic malignant melanomas. Int J Cancer *109*: 377-384, 2004.

2 Lito P, Pratilas CA, Joseph EW, Tadi M, Halilovic E, Zubrowski M, Huang A, Wong WL, Callahan MK, Merghoub T, Wolchok JD, de Stanchina E, Chandarlapaty S, Poulikakos PI, Fagin JA and Rosen N: Relief of profound feedback inhibition of mitogenic signaling by RAF inhibitors attenuates their activity in *BRAF*V600E melanomas. Cancer Cell *22*: 668-682, 2012.

3 Davies H, Bignell GR, Cox C, Stephens P, Edkins S, Clegg S, Teague J, Woffendin H, Garnett MJ, Bottomley W, Davis N, Dicks E, Ewing R, Floyd Y, Gray K, Hall S, Hawes R, Hughes J, Kosmidou V, Menzies A, Mould C, Parker A, Stevens C, Watt S, Hooper S, Wilson R, Jayatilake H, Gusterson BA, Cooper C, Shipley J, Hargrave D, Pritchard-Jones K, Maitland N, Chenevix-Trench G, Riggins GJ, Bigner DD, Palmieri G, Cossu A, Flanagan A, Nicholson A, Ho JW, Leung SY, Yuen ST, Weber BL, Seigler HF, Darrow TL, Paterson H, Marais R, Marshall CJ, Wooster R, Stratton MR and Futreal PA: Mutations of the BRAF gene in human cancer. Nature *417*: 949-954, 2002.

4 Calipel A, Lefevre G, Pouponnot C, Mouriaux F, Eychene A and Mascarelli F: Mutation of *BRAF* in human choroidal melanoma cells mediates cell proliferation and transformation through the MEK/ERK pathway. J Biol Chem *278*: 42409-42418, 2003.

5 Manzano JL, Layos L, Buges C, de Los Llanos Gil M, Vila L, Martinez-Balibrea E and Martinez-Cardus A: Resistant mechanisms to BRAF inhibitors in melanoma. Ann Transl Med *4*: 237, 2016.

6 Wahid M, Jawed A, Mandal RK, Dar SA, Akhter N, Somvanshi P, Khan F, Lohani M, Areeshi MY and Haque S: Recent developments and obstacles in the treatment of melanoma with BRAF and MEK inhibitors. Crit Rev Oncol Hematol *125*: 84-88, 2018.

7 Le K, Blomain ES, Rodeck U and Aplin AE: Selective RAF inhibitor impairs ERK1/2 phosphorylation and growth in mutant NRAS, vemurafenib-resistant melanoma cells. Pigment Cell Melanoma Res *26*: 509-517, 2013.

8 Johnson DB, Childress MA, Chalmers ZR, Frampton GM, Ali SM, Rubinstein SM, Fabrizio D, Ross JS, Balasubramanian S, Miller VA, Stephens PJ, Sosman JA and Lovly CM: *BRAF* internal deletions and resistance to BRAF/MEK inhibitor therapy. Pigment Cell Melanoma Res *31*: 432-436, 2018.

9 Tran KA, Cheng MY, Mitra A, Ogawa H, Shi VY, Olney LP, Kloxin AM and Maverakis E: MEK inhibitors and their potential in the treatment of advanced melanoma: the advantages of combination therapy. Drug Des Devel Ther *10*: 43-52, 2016.

10 Mazzio EA and Soliman KF: Basic concepts of epigenetics: The impact of environmental signals on gene expression. Epigenetics *7*: 119-130, 2012.

11 Gallagher SJ, Tiffen JC and Hersey P: Histone modifications, modifiers, and readers in melanoma resistance to targeted and immune therapy. Cancers (Basel) *7*: 1959-1982, 2015.

12 Krumm A, Barckhausen C, Kucuk P, Tomaszowski KH, Loquai C, Fahrer J, Kramer OH, Kaina B and Roos WP: Enhanced histone deacetylase activity in malignant melanoma provokes RAD51 and FANCD2-triggered drug Resistance. Cancer Res *76*: 3067-3077, 2016.

13 Hornig E, Heppt MV, Graf SA, Ruzicka T and Berking C: Inhibition of histone deacetylases in melanoma-a perspective from bench to bedside. Exp Dermatol *25*: 831-838, 2016.

14 Jonas O, Oudin MJ, Kosciuk T, Whitman M, Gertler FB, Cima MJ, Flaherty KT and Langer R: Parallel *in vivo* assessment of drug phenotypes at various time points during systemic BRAF inhibition reveals tumor adaptation and altered treatment vulnerabilities. Clin Cancer Res *22*: 6031-6038, 2016.

15 Lai F, Guo ST, Jin L, Jiang CC, Wang CY, Croft A, Chi MN, Tseng HY, Farrelly M, Atmadibrata B, Norman J, Liu T, Hersey P and Zhang XD: Cotargeting histone deacetylases and oncogenic BRAF synergistically kill human melanoma cells by necrosis independently of RIPK1 and RIPK3. Cell Death Dis *4*: e655, 2013.

16 Wilmott JS, Colebatch AJ, Kakavand H, Shang P, Carlino MS, Thompson JF, Long GV, Scolyer RA and Hersey P: Expression of the class 1 histone deacetylases HDAC8 and 3 are associated with improved survival of patients with metastatic melanoma. Mod Pathol *28*: 884-894, 2015.

17 Dai W, Zhou J, Jin B and Pan J: Class III-specific HDAC inhibitor Tenovin-6 induces apoptosis, suppresses migration and eliminates cancer stem cells in uveal melanoma. Sci Rep *6*: 22622, 2016.
18 Venza I, Visalli M, Oteri R, Teti D and Venza M: Class I-specific histone deacetylase inhibitor MS-275 overrides TRAIL-resistance in melanoma cells by downregulating c-FLIP. Int Immunopharmacol *21*: 439-446, 2014.
19 Huang da W, Sherman BT and Lempicki RA: Bioinformatics enrichment tools: paths toward the comprehensive functional analysis of large gene lists. Nucleic Acids Res *37*: 1-13, 2009.
20 Garmpis N, Damaskos C, Garmpi A, Dimitroulis D, Spartalis E, Margonis GA, Schizas D, Deskou I, Doula C, Magkouti E, Andreatos N, Antoniou EA, Nonni A, Kontzoglou K and Mantas D: Targeting histone deacetylases in malignant melanoma: A future therapeutic agent or just great expectations? Anticancer Res *37*: 5355-5362, 2017.
21 Ibrahim N, Buchbinder EI, Granter SR, Rodig SJ, Giobbie-Hurder A, Becerra C, Tsiaras A, Gjini E, Fisher DE and Hodi FS: A phase I trial of panobinostat (LBH589) in patients with metastatic melanoma. Cancer Med *5*: 3041-3050, 2016.
22 Yao L, Wang L, Li F, Gao X, Wei X and Liu Z: MiR181c inhibits ovarian cancer metastasis and progression by targeting PRKCD expression. Int J Clin Exp Med *8*: 15198-15205, 2015.
23 Abe Y, Nagano M, Kuga T, Tada A, Isoyama J, Adachi J and Tomonaga T: Deep phospho-and phosphotyrosine proteomics identified active kinases and phosphorylation networks in colorectal cancer cell lines resistant to cetuximab. Sci Rep *7*: 10463, 2017.
24 Zuo Y, Wu Y and Chakraborty C: CDC42 negatively regulates intrinsic migration of highly aggressive breast cancer cells. J Cell Physiol *227*: 1399-1407, 2012.
25 Chauvin L, Goupille C, Blanc C, Pinault M, Domingo I, Guimaraes C, Bougnoux P, Chevalier S and Maheo K: Long chain n-3 polyunsaturated fatty acids increase the efficacy of docetaxel in mammary cancer cells by down-regulating AKT and PKCepsilon/delta-induced ERK pathways. Biochim Biophys Acta *1861*: 380-390, 2016.
26 Chen CL, Wang SH, Chan PC, Shen MR and Chen HC: Phosphorylation of E-cadherin at threonine 790 by protein kinase Cdelta reduces beta-catenin binding and suppresses the function of E-cadherin. Oncotarget *7*: 37260-37276, 2016.
27 Kim H, Na YR, Kim SY and Yang EG: Protein kinase C isoforms differentially regulate hypoxia-inducible factor-1alpha accumulation in cancer cells. J Cell Biochem *117*: 647-658, 2016.
28 Zhu S, Yao F, Li WH, Wan JN, Zhang YM, Tang Z, Khan S, Wang CH and Sun SR: PKCδ-dependent activation of the ubiquitin proteasome system is responsible for high glucose-induced human breast cancer MCF-7 cell proliferation, migration, and invasion. Asian Pac J Cancer Prev *14*: 5687-5692, 2013.
29 Singleton KR, Crawford L, Tsui E, Manchester HE, Maertens O, Liu X, Liberti MV, Magpusao AN, Stein EM, Tingley JP, Frederick DT, Boland GM, Flaherty KT, McCall SJ, Krepler C, Sproesser K, Herlyn M, Adams DJ, Locasale JW, Cichowski K, Mukherjee S and Wood KC: Melanoma therapeutic strategies that select against resistance by exploiting MYC-driven evolutionary convergence. Cell Rep *21*: 2796-2812, 2017.
30 Kfoury A, Armaro M, Collodet C, Sordet-Dessimoz J, Giner MP, Christen S, Moco S, Leleu M, de Leval L, Koch U, Trumpp A, Sakamoto K, Beermann F and Radtke F: AMPK promotes survival of c-MYC-positive melanoma cells by suppressing oxidative stress. EMBO J 37(5), 2018. doi: 10.15252/embj.201797673.
31 Korkut A, Wang W, Demir E, Aksoy BA, Jing X, Molinelli EJ, Babur O, Bemis DL, Onur Sumer S, Solit DB, Pratilas CA and Sander C: Perturbation biology nominates upstream-downstream drug combinations in RAF inhibitor resistant melanoma cells. Elife 4, 2015. doi: 10.7554/eLife.04640.
32 Liu D, Liu X and Xing M: Activities of multiple cancer-related pathways are associated with *BRAF* mutation and predict the resistance to BRAF/MEK inhibitors in melanoma cells. Cell Cycle *13*: 208-219, 2014.
33 Qu X, Shen L, Zheng Y, Cui Y, Feng Z, Liu F and Liu J: A signal transduction pathway from TGF-beta1 to SKP2 *via* AKT1 and c-MYC and its correlation with progression in human melanoma. J Invest Dermatol *134*: 159-167, 2014.
34 Mahapatra L, Andruska N, Mao C, Le J and Shapiro DJ: A novel IMP1 inhibitor, BTYNB, targets c-MYC and inhibits melanoma and ovarian cancer cell proliferation. Transl Oncol *10*: 818-827, 2017.
35 Chen Y, Bathula SR, Yang Q and Huang L: Targeted nanoparticles deliver siRNA to melanoma. J Invest Dermatol *130*: 2790-2798, 2010.
36 Dorasamy MS, Choudhary B, Nellore K, Subramanya H and Wong PF: Dihydroorotate dehydrogenase inhibitors target c-MYC and arrest melanoma, myeloma and lymphoma cells at S-phase. J Cancer *8*: 3086-3098, 2017.
37 Zhang F, Shen M, Yang L, Yang X, Tsai Y, Keng PC, Chen Y, Lee SO and Chen Y: Simultaneous targeting of ATM and MCL-1 increases cisplatin sensitivity of cisplatin-resistant non-small cell lung cancer. Cancer Biol Ther *18*: 606-615, 2017.
38 Stolz A, Ertych N and Bastians H: Tumor suppressor CHK2: A regulator of DNA damage response and mediator of chromosomal stability. Clin Cancer Res *17*: 401-405, 2011.
39 Squatrito M, Brennan CW, Helmy K, Huse JT, Petrini JH and Holland EC: Loss of ATM/CHK2/p53 pathway components accelerates tumor development and contributes to radiation resistance in gliomas. Cancer Cell *18*: 619-629, 2010.
40 Wang W, Nacusi L, Sheaff RJ and Liu X: Ubiquitination of P21CIP1/WAF1 by SCFSKP2: substrate requirement and ubiquitination site selection. Biochemistry *44*: 14553-14564, 2005.
41 Gstaiger M, Jordan R, Lim M, Catzavelos C, Mestan J, Slingerland J and Krek W: SKP2 is oncogenic and overexpressed in human cancers. Proc Natl Acad Sci USA *98*: 5043-5048, 2001.
42 Li P, Li C, Zhao X, Zhang X, Nicosia SV and Bai W: p27(KIP1) stabilization and G(1) arrest by 1,25-dihydroxyvitamin D(3) in ovarian cancer cells mediated through down-regulation of cyclin E/cyclin-dependent kinase 2 and SKP1-Cullin-F-box protein/SKP2 ubiquitin ligase. J Biol Chem *279*: 25260-25267, 2004.
43 Bornstein G, Bloom J, Sitry-Shevah D, Nakayama K, Pagano M and Hershko A: Role of the SCFSKP2 ubiquitin ligase in the degradation of P21CIP1 in S phase. J Biol Chem *278*: 25752-25757, 2003.
44 Nakamura Y, Ozaki T, Koseki H, Nakagawara A and Sakiyama S: Accumulation of p27 KIP1 is associated with BMP2-induced growth arrest and neuronal differentiation of human neuroblastoma-derived cell lines. Biochem Biophys Res Commun *307*: 206-213, 2003.

45 Ang XL and Harper JW: Interwoven ubiquitination oscillators and control of cell cycle transitions. Sci STKE *2004*: pe31, 2004.
46 Sun J, Shi R, Zhao S, Li X, Lu S, Bu H and Ma X: Cell division cycle 45 promotes papillary thyroid cancer progression *via* regulating the cell cycle. Tumour Biol *39*: 1010428317705342, 2017.
47 Xu Y, Gristwood T, Hodgson B, Trinidad JC, Albers SV and Bell SD: Archaeal orthologs of Cdc45 and GINS form a stable complex that stimulates the helicase activity of MCM. Proc Natl Acad Sci USA *113*: 13390-13395, 2016.
48 Yabuuchi H, Yamada Y, Uchida T, Sunathvanichkul T, Nakagawa T and Masukata H: Ordered assembly of SLD3, GINS, and CDC45 is distinctly regulated by DDK and CDK for activation of replication origins. EMBO J *25*: 4663-4674, 2006.
49 Chen H, Xu X, Wang G, Zhang B, Wang G, Xin G, Liu J, Jiang Q, Zhang H and Zhang C: CDK4 protein is degraded by anaphase-promoting complex/cyclosome in mitosis and reaccumulates in early G1 phase to initiate a new cell cycle in HeLa cells. J Biol Chem *292*: 10131-10141, 2017.
50 Jing Y, Wang G, Ge Y, Xu M, Tang S and Gong Z: AA-PMe, a novel asiatic acid derivative, induces apoptosis and suppresses proliferation, migration, and invasion of gastric cancer cells. Onco Targets Ther *9*: 1605-1621, 2016.
51 Choi YH: Induction of apoptosis by trichostatin A, a histone deacetylase inhibitor, is associated with inhibition of cyclooxygenase-2 activity in human non-small cell lung cancer cells. Int J Oncol *27*: 473-479, 2005.
52 Vanhaecke T, Henkens T, Kass GE and Rogiers V: Effect of the histone deacetylase inhibitor trichostatin A on spontaneous apoptosis in various types of adult rat hepatocyte cultures. Biochem Pharmacol *68*: 753-760, 2004.
53 Duan H, Heckman CA and Boxer LM: Histone deacetylase inhibitors down-regulate BCL-2 expression and induce apoptosis in t(14;18) lymphomas. Mol Cell Biol *25*: 1608-1619, 2005.
54 Ansari MF, Idrees D, Hassan MI, Ahmad K, Avecilla F and Azam A: Design, synthesis and biological evaluation of novel pyridine-thiazolidinone derivatives as anticancer agents: Targeting human carbonic anhydrase IX. Eur J Med Chem *144*: 544-556, 2018.
55 Queen A, Khan P, Idrees D, Azam A and Hassan MI: Biological evaluation of p-toluene sulphonylhydrazone as carbonic anhydrase IX inhibitors: An approach to fight hypoxia-induced tumors. Int J Biol Macromol *106*: 840-850, 2018.
56 Puech C, Chatard M, Felder-Flesch D, Prevot N and Perek N: Umbelliferone decreases intracellular pH and sensitizes melanoma cell line A375 to dacarbazin. Comparison with acetazolamide. Curr Mol Pharmacol *11(2)*: 133-139, 2016.
57 Federici C, Lugini L, Marino ML, Carta F, Iessi E, Azzarito T, Supuran CT and Fais S: Lansoprazole and carbonic anhydrase IX inhibitors sinergize against human melanoma cells. J Enzyme Inhib Med Chem *31*: 119-125, 2016.
58 Bayat Mokhtari R, Baluch N, Ka Hon Tsui M, Kumar S, T SH, Aitken K, Das B, Baruchel S and Yeger H: Acetazolamide potentiates the anti-tumor potential of HDACi, MS-275, in neuroblastoma. BMC Cancer *17*: 156, 2017.
59 Yan C, Kim YH, Kang HW, Seo SP, Jeong P, Lee IS, Kim D, Kim JM, Choi YH, Moon SK, Yun SJ and Kim WJ: Urinary nucleic acid TSPAN13-to-S100A9 ratio as a diagnostic marker in prostate cancer. J Korean Med Sci *30*: 1784-1792, 2015.
60 Arencibia JM, Martin S, Perez-Rodriguez FJ and Bonnin A: Gene expression profiling reveals overexpression of TSPAN13 in prostate cancer. Int J Oncol *34*: 457-463, 2009.
61 Mi H, Muruganujan A and Thomas PD: PANTHER in 2013: Modeling the evolution of gene function, and other gene attributes, in the context of phylogenetic trees. Nucleic Acids Res *41*: D377-386, 2013.
62 Gaudet P, Livstone MS, Lewis SE and Thomas PD: Phylogenetic-based propagation of functional annotations within the Gene Ontology consortium. Brief Bioinform *12*: 449-462, 2011.

Received June 8, 2018
Revised July 9, 2018
Accepted July 16, 2018